Contents lists available at SciOpen

Food Science and Human Wellness

journal homepage: https://www.sciopen.com/journal/2097-0765

China Food Publishing Co.

Farrerol as an innovative antivirulence agent disrupting virulence factors to combat foodborne pathogenicity in *Staphylococcus aureus*

Hangqian Yu[a,b,1], Yuxin Zhang[c,1], Yuxin Yang[d], Xiaoping Zhou[d], Dacheng Wang[b,*]

[a] State Key Laboratory for Diagnosis and Treatment of Severe Zoonotic Infectious Diseases, Key Laboratory for Zoonosis Research of the Ministry of Education, College of Veterinary Medicine, Jilin University, Changchun 130062, China
[b] College of Animal Science, Jilin University, Changchun 130062, China
[c] College of Basic Medical Sciences, Jilin University, Changchun 130021, China
[d] School of Pharmaceutical Science, Jilin University, Changchun 130021, China

ARTICLE INFO

Article history:
Received 1 August 2024
Received in revised form 12 September 2024
Accepted 17 October 2024

Keywords:
Foodborne *Staphylococcus aureus*
Farrerol
Drug resistance
Caseinolytic peptidase P

ABSTRACT

The overuse of antibiotics has accelerated the emergence of resistant bacteria, posing critical threats to food safety and public health. This challenge underscores the urgent need for alternative strategies, such as antivirulence therapy, which disarms pathogens by targeting virulence factors rather than inhibiting bacterial growth. In this study, we identified farrerol, a flavonoid, as a potent inhibitor of the caseinolytic peptidase P (ClpP) protease, a key virulence regulator in *Staphylococcus aureus*, with an IC_{50} of 19.33 μg/mL. Farrerol significantly disrupts virulence factor secretion and reduces pathogenicity, demonstrating its potential to control *S. aureus*-induced foodborne illnesses. Mechanistic studies using fluorescence resonance energy transfer (FRET), thermal shift assay (TSA), cellular thermal shift assay (CETSA), fluorescence quenching, and molecular docking revealed that farrerol interacts with ClpP *via* key residues (GLY-127, GLN-132, and ASP-170). *In vivo*, farrerol reduced the bacterial load and improved survival in a *Galleria mellonella* infection model. Our findings demonstrated that farrerol is an effective antivirulence agent, offering an innovative approach for the food industry to control *S. aureus*-induced foodborne infections. This approach holds great potential for enhancing food safety and mitigating antibiotic resistance.

1. Introduction

Foodborne *Staphylococcus aureus* is a significant public health concern due to its prevalence and severe health risks[1-2]. This pathogen is responsible for numerous outbreaks of food poisoning worldwide and is characterized by symptoms such as nausea, vomiting, abdominal cramps, and diarrhea[3].

Globally, foodborne pathogens are among the leading causes of food contamination, contributing to both food spoilage and the transmission of disease, with substantial economic repercussions. The World Health Organization (WHO) estimates that foodborne diseases affect 600 million individuals and result in 420 000 deaths annually, leading to over $100 billion in global economic losses[4]. These pathogens not only threaten consumer health but also impose a significant burden on the food industry, with foodborne *S. aureus* standing out as a prominent contributor to these global challenges[5]. In the United States alone, *S. aureus* accounts for an estimated 241 000 cases of foodborne illness annually[6]. This pathogen is commonly found in a variety of foods, including dairy products, meats, poultry, and prepared foods such as salads and sandwiches[7-8]. The prevalence of *S. aureus* contamination in different food categories varies across studies and regions. In raw milk, contamination rates range from

[1] These authors contributed equally to this work.
* Corresponding author at: College of Animal Science, Jilin University, Changchun 130062, China.
E-mail address: wangdc@jlu.edu.cn (D.C. Wang)
Peer review under responsibility of Beijing Academy of Food Sciences.

Sciopen Publishing services by Tsinghua University Press

http://doi.org/10.26599/FSHW.2024.9250429

12.8% in Iran to as high as 75% in Norway[9]. A study in Northern Xinjiang, China, reported a prevalence of 43.1% in raw retail milk, with cow milk samples showing the highest contamination of 61.7%[10]. In dairy and beef production environments, the prevalence of *S. aureus* in raw milk and beef products has been reported ranging from 17.5% to 48.7%, depending on factors such as geographic location, hygiene practices, and the use of antimicrobials[11]. In the meat supply chain, contamination rates in beef, pork, and poultry have been reported ranging from 17.5% to 42.9%, with the highest prevalence observed in beef from USA (37%) and Italy (29.41%)[11]. The impact of foodborne pathogens, including *S. aureus*, extends beyond public health concerns, contributing to significant economic losses due to medical expenses, lost productivity, and food recalls. Despite ongoing efforts to combat foodborne *S. aureus* infections, current food safety measures still face challenges in addressing this issue effectively. Innovative strategies are needed to mitigate the impact of this pathogen on global health and the food industry.

The ability of *S. aureus* to cause disease is largely attributed to its production of a variety of virulence factors, which facilitate its colonization, immune evasion, and tissue damage. Antivirulence therapy, which targets the virulence factors of pathogens rather than their viability, represents a promising alternative to traditional antibiotics[12-15]. This strategy minimizes the selective pressure for resistance development and preserves the host microbiota. In the food industry, the application of antivirulence agents can increase food safety by reducing the pathogenicity of contaminants without affecting beneficial microorganisms. Recent studies have highlighted the potential of antivirulence agents for controlling foodborne pathogens, including the use of natural compounds and small molecules to inhibit virulence factors. For example, eugenol, a natural compound, effectively inhibits CrtM, an enzyme essential for the biosynthesis of staphyloxanthin in *S. aureus*. By disrupting staphyloxanthin production, eugenol compromises the bacterium's defense against oxidative stress and immune responses, thereby attenuating its virulence and improving the control of contamination in food products. Similarly, 3,3′-diindolylmethane (DIM) has demonstrated potent antibiofilm activity, preventing biofilm formation on food-contact surfaces[4]. This not only impairs *S. aureus* persistence but also enhances the efficacy of disinfectants, reinforcing hygiene standards in food processing environments. These studies underscore the promising role of antivirulence strategies in mitigating the risks of *S. aureus* contamination and advancing food safety practices.

Among the virulence factors of *S. aureus*, caseinolytic peptidase P (ClpP) plays a crucial role. ClpP is a highly conserved protease that contributes to the pathogenicity of *S. aureus* by degrading misfolded proteins and regulating the expression of other virulence determinants[16-17]. ClpP not only helps in the survival of bacteria under stress conditions but also modulates the bacterial proteome in a way that enhances virulence. Targeting ClpP represents a novel therapeutic strategy to mitigate the virulence of *S. aureus* without necessarily killing the bacteria, thus potentially reducing the selective pressure for the development of antibiotic resistance. ClpP regulates several key factors and pathways in *S. aureus*, including the accessory gene regulator (agr) quorum-sensing system and the staphylococcal accessory regulator (sarA) family of transcriptional regulators[18-20]. The agr system controls the expression of toxins and enzymes that contribute to the ability of bacteria to cause disease, and ClpP modulates this system by degrading specific regulatory proteins, influencing the production of virulence factors, such as α-hemolysin and Panton-Valentine leukocidin (PVL)[21]. Additionally, ClpP impacts the sarA family of regulators, which are essential for the expression of various virulence genes. Studies have highlighted the importance of ClpP in these regulatory networks, underscoring its potential as a target for antivirulence therapies.

Recent research from our laboratory has identified farrerol as a compound with promising potential to inhibit the virulence factor ClpP in foodborne *S. aureus*. Farrerol is a natural product extracted from the plant species *Rhododendron* that is known for its medicinal properties. It has been traditionally used in herbal medicine for its anti-inflammatory and analgesic effects[22-23]. In our study, we demonstrated that farrerol significantly inhibited the activity of ClpP in *S. aureus*, leading to a marked reduction in bacterial virulence. Furthermore, we elucidated the direct interaction between farrerol and ClpP, which contributes to the protective effects of farrerol observed in the *Galleria mellonella* model of MRSA infection. Our key findings highlight the potential of farrerol as an antivirulence agent, offering a novel therapeutic strategy that disarms pathogens without promoting resistance. This approach shows great promise for mitigating foodborne illnesses associated with *S. aureus* and contributes to broader efforts in combating antibiotic resistance.

2. Materials and methods

2.1 Bacterial strains, plasmids, culture conditions, and reagents

S. aureus USA300 (USA300-HOU-MR) was utilized, with cultures maintained at 37 °C and agitated at 180 r/min. *Escherichia coli* strains were cultured in Luria Bertani (LB) broth or on LB agar plates from Hopebio (Qingdao, China), while *S. aureus* strains were grown in tryptic soy broth (TSB) or on tryptic soy agar. For plasmid selection, 50 μg/mL kanamycin was used for *E. coli*. The farrerol compound (CAS No. 2411-30-1, 99% purity; Chengdu Pufeide Biotech Co., Ltd., China) was dissolved in dimethyl sulfoxide (DMSO) to create a 10 mg/mL stock solution.

2.2 Protein expression and purification

Proteins were expressed in the *E. coli* BL21 (DE_3) strain. The BL21 strain containing the pET28a-*clpP* plasmid was cultured in LB broth supplemented with 50 μg/mL kanamycin. When the absorbance at 600 nm reached 0.6, protein expression was induced with 0.5 mmol/L isopropyl-*β*-*D*-thiogalactopyranoside (IPTG), followed by overnight incubation at 20 °C with shaking at 160 r/min. The cells were harvested, resuspended in lysis buffer (40 mmol/L Tris, pH 8.5), and lysed *via* sonication. The lysate was centrifuged at 12 000 r/min for 1 h at 4 °C, and the supernatant was applied to a His-Trap column (GE Healthcare). The ClpP protein was eluted with a gradient of imidazole and confirmed by SDS-PAGE.

Using the pET28a-*clpP* plasmid as a template and the mutagenic primers listed in Supplementary Table 1, site-directed mutagenesis was performed with a Tiangen Fast Mutagenesis Kit (KM101, Tiangen, China). The mutant proteins were expressed and purified following the same protocol used for the wild-type protein.

2.3 Screening of ClpP inhibitors

The intrinsic hydrolytic activity of ClpP was utilized to screen for potential inhibitors using a FRET-based assay. A black opaque 96-well plate containing 10 μmol/L ClpP and 64 μg/mL test compound in 100 μL of ClpP buffer (100 mmol/L HEPES, 100 mmol/L NaCl) was set up. This mixture was incubated for 1 h at room temperature to allow any interactions between ClpP and the compound. Following this incubation, 10 μmol/L Suc-LeuTyr-AMC (Cat No. S1153, Sigma-Aldrich, St. Louis, MO, USA) was added to each well. The plates were then incubated at 32 °C for an additional 30 min to enable the hydrolytic reaction. Fluorescence was measured *via* a TECAN spark with an excitation wavelength of 360 nm and an emission wavelength of 465 nm to quantify the hydrolytic activity and assess the inhibitory effect of the compound.

2.4 Resazurin microtiter assay

The minimum inhibitory concentration (MIC) was determined *via* the broth microdilution method according to the Clinical and Laboratory Standards Institute (CLSI) guidelines. In brief, 1×10^5 *S. aureus* cells were inoculated into 100 μL of cation-adjusted Mueller-Hinton broth (CAMHB) in a 96-well plate. Serial dilutions of farrerol were added along with 2 μL of 0.1% resazurin solution to each well. The plates were incubated for 16 h at 37 °C. The MIC was determined by observing the color change from blue to pink, indicating bacterial growth.

2.5 Growth assay

For the growth inhibition assays, *S. aureus* USA300 was inoculated into TSB containing 32 μg/mL of farrerol. The bacterial cultures were incubated with continuous shaking, and optical density at 600 nm ($OD_{600\ nm}$) was measured at regular intervals over a 24-h period. This approach allowed for precise monitoring of the inhibitory effects of farrerol on bacterial growth kinetics.

2.6 Cytotoxicity assay

The cytotoxicity of farrerol (0–32 μg/mL) on A549 cells (a human lung carcinoma cell line) and L929 cells (mouse fibroblast cells) was evaluated using the MTT assay, following the manufacturer's instructions. A549 and L929 cells (2×10^4 cells/well) were seeded in 96-well plates and incubated for 24 h prior to the addition of 100 μL of farrerol-containing DMEM medium. After 24 h of treatment, the medium was replaced with 100 μL of MTT solution (0.5 mg/mL), and the cells were incubated for an additional 4 h at 37 °C. The MTT solution was then removed, and the resulting formazan crystals were dissolved in 100 μL of DMSO. OD was measured at 490 nm to assess cell viability.

2.7 RNA extraction and quantitative PCR

S. aureus was grown in TSB until $OD_{600\ nm}$ reached 0.3. At this stage, farrerol was added to the culture at a final concentration of 32 μg/mL. Following incubation, the bacterial cells were harvested, and total RNA was extracted using the TRIzol method. The RNA was then reverse-transcribed into cDNA using the PrimeScript RT reagent kit (Cat No. RR047Q, TaKaRa). Quantitative PCR (qPCR) was conducted on an ABI 7900HT real-time PCR system to analyze gene expression levels. The relative transcript levels were normalized to the 16S rRNA gene, which served as an internal control. This process was performed in triplicate to ensure reproducibility. Primer sequences used in the qPCR assays are provided in Table S2.

2.8 Western blot analysis

Proteins extracted from *S. aureus* cultures treated with varying concentrations of farrerol were separated by 12% SDS-PAGE and transferred onto PVDF membranes (Millipore, USA). The membranes were blocked with a suitable blocking buffer to prevent nonspecific binding and then incubated with primary antibodies. The primary antibodies used were anti-alpha-toxin (1:4 000 dilution, Cat No. S7531, Sigma-Aldrich, USA) and anti-PVL LukS subunit (1:4 000 dilution, Cat No. ab190473, Abcam, UK). Following incubation with the primary antibodies, the membranes were treated with an HRP-conjugated goat anti-rabbit IgG secondary antibody (1:5 000 dilution, Cat No. SE134, Solarbio, Beijing, China). Protein bands were visualized using a chemiluminescent substrate and quantified using ImageJ software.

2.9 Hemolysis assay

S. aureus cultures were grown in TSB and treated with graded concentrations of farrerol (4, 8, 16, and 32 μg/mL) until the $OD_{600\ nm}$ reached 2.5. The supernatants were collected, filtered to remove cellular debris, and 100 μL of each was mixed with 875 μL phosphate-buffered saline (PBS) and 25 μL defibrinated rabbit blood. These mixtures were incubated at 37 °C for 30 min, after which they were centrifuged to further eliminate any remaining cells or debris. Hemolysis was assessed by measuring the absorbance of the supernatant at 543 nm, which reflects the release of hemoglobin. PBS was used as the positive control to ensure accurate baseline measurements of hemolytic activity.

2.10 Plate hemolysis

For the hemolysis assay, TSB agar plates supplemented with 5% defibrinated rabbit blood were prepared in advance. *S. aureus* cultures, treated either with DMSO or 32 μg/mL farrerol, were diluted to an $OD_{600\ nm}$ of 0.1. A volume of 2.5 μL of each diluted culture was then spotted onto the blood agar plates. The ClpP knockout strain served as a control. The plates were incubated overnight at 37 °C, allowing for bacterial growth and hemolytic activity. The following day, the formation of clear zones around the bacterial colonies, indicative of hemolysis, was carefully observed and quantitatively recorded.

2.11 Urease activity analysis

The production of urease by *S. aureus* was evaluated using a urease agar base medium (Cat. No. HB4095, Hopebio, Qingdao, China) containing phenol red as a pH indicator. *S. aureus* cultures were inoculated into the medium, and farrerol (32 μg/mL) was added to assess its effect on urease activity. The color change of the medium,

reflecting urease activity, was monitored over a 2-day period. Additionally, agar blocks were appropriately weighed and dissolved for spectrophotometric analysis. The absorbance was measured across a continuous wavelength range using a spectrophotometer (Thermo Fisher Scientific, USA) to further quantify the urease activity.

2.12 Invasion assay via fluorescence microscopy

A549 cells were seeded into 24-well plates and infected with *S. aureus* at an $OD_{600\ nm}$ of 1.0, with a bacteria-to-cell ratio of 20:1. After a 1-h incubation period to allow bacterial invasion, the cells were washed with PBS to remove any nonadherent bacteria. Gentamicin (300 μg/mL) was then added to the wells for 2 h to eradicate extracellular bacteria. Bacterial cells were stained with 5(6)-FAM SE, the cytoskeleton was labeled using phalloidin, and nuclei were counterstained with DAPI. This staining protocol enabled detailed visualization of bacterial invasion through fluorescence microscopy. Additionally, serial dilutions of the cell lysates were plated onto agar and incubated overnight at 37 °C to allow the formation of distinct bacterial colonies.

2.13 Thermal shift assay (TSA)

Direct binding of natural compounds to target proteins is crucial for their inhibitory effects. In this study, a TSA was employed to evaluate the impact of farrerol on the thermal stability of the ClpP protein. ClpP (2 μmol/L) was mixed with TSA buffer (150 mmol/L NaCl, 10 mmol/L HEPES, pH 7.5), 32 μg/mL farrerol, and SYPRO Orange dye (Cat. No. S5692; Sigma-Aldrich, USA). The control group received an equivalent volume of DMSO. The mixture was gradually heated from 25 to 90 °C at a rate of 1 °C/min. Changes in fluorescence were monitored *via* the Bio-Rad iQ5 system, allowing for the determination of the protein's thermal denaturation profile.

2.14 Cellular thermal shift assay (CETSA)

Lysates from *E. coli* expressing ClpP were used to investigate the binding of farrerol to ClpP *via* a CETSA. The lysates were incubated with either farrerol or DMSO as a control. After incubation, the samples were subjected to heat treatment (25–65 °C), followed by centrifugation to separate the soluble proteins from the precipitated fraction. The supernatants were analyzed by SDS-PAGE, and the gels were stained with Coomassie blue. Band intensities were quantified *via* ImageJ software to determine the thermal stability of ClpP in the presence of farrerol.

2.15 Fluorescence quenching analysis

The ClpP protein was first extracted, and its concentration was measured. The protein was then diluted to 500 μg/mL in PBS, and farrerol was prepared at a concentration of 0.5 mg/mL. The RFPC program was employed for the fluorescence quenching assay with the following parameters: emission wavelength set at 326 nm and an excitation wavelength range of 280–400 nm (broad-spectrum fluorescence emission scan). After washing the quartz cuvette with PBS, 2 mL of the diluted ClpP protein was added to achieve an initial fluorescence intensity of approximately 800 units. Farrerol was gradually added to the cuvette in small volumes, and each addition's effect on fluorescence intensity was recorded, specifically noting the volume required to reduce the fluorescence intensity by 50–100 units. The corresponding fluorescence emission spectra were exported using a fluorescence spectrophotometer. The titration continued until no significant reduction in fluorescence intensity was observed with further farrerol addition. Finally, a plot of fluorescence intensity versus the increasing volume (concentration) of farrerol was generated to determine the binding constant (K_A).

2.16 Surface plasmon resonance (SPR) analysis

The SPR experiment was performed *via* the OpenSPR™ (Nicoya) instrument. First, an activator solution was prepared by mixing 400 mmol/L EDC and 100 mmol/L NHS immediately before injection. The chip was activated with this mixture for 240 s at a flow rate of 20 μL/min. ClpP was then diluted to 60 μg/mL in immobilization buffer and injected into the sample channel at the same flow rate. Following immobilization, the chip was deactivated with 1 mol/L ethanolamine hydrochloride and injected at 20 μL/min for 240 s. Farrerol was prepared in analyte buffer at 6 concentrations (0, 10, 20, 40, 80, and 160 μmol/L). Each concentration was injected into the sample channel at a flow rate of 20 μL/min, with a 240 s association phase and a 360 s dissociation phase. A series of 6 analyte injections were performed in ascending concentration order. After each cycle, the sensor chip surface was regenerated with 10 mmol/L glycine-HCl at 150 μL/min for 10 s to remove the analyte. This process was repeated for each concentration of farrerol.

2.17 Molecular docking

To explore the potential binding mode between farrerol and ClpP, molecular docking was conducted *via* AutoDock Vina software. Molecular simulations were conducted to explore the primary amino acid residues involved in the binding of farrerol to ClpP. The crystal structure of ClpP (PDB ID: 3V5E) was sourced from the Protein Data Bank. The 3D structure of farrerol was generated *via* ChemBioDraw Ultra. Preparation for docking was performed with AutoDockTools, which included merging nonpolar hydrogen atoms and specifying rotatable bonds in the ligand structures. Default parameters were employed for Vina docking unless stated otherwise. Subsequently, molecular dynamics (MD) simulations were carried out to refine the docking results.

2.18 MD simulation and calculation of the binding free energy

MD simulations of the selected docked poses were conducted *via* the Amber 14 and AmberTools 15 programs. The ligand topology file was generated with the AMBER front field *via* the ACPYPE script, while the AMBER99SB-ILDN force field was used for the protein topology file. The system was solvated in a rectangular box with a 10.0 Å boundary of TIP3P water, utilizing the "SolvateOct" command to ensure a minimum distance between any solute atoms. Equilibration of the solvated complex involved a brief minimization (500 steps each of steepest descent and conjugate gradient methods), followed by 500 ps of heating and 50 ps of density equilibration with weak restraints using the GPU-accelerated PMEMD (Particle

Mesh Ewald Molecular Dynamics) module on an NVIDIA® Tesla K20c. Finally, 100 ns of MD simulations were performed on a Dell Precision T5500 workstation. The stability of the protein and the complex system was assessed *via* the root mean square deviation (RMSD), which indicates the degree of molecular structure change. The root mean square fluctuation (RMSF) and radius of gyration (Rg) were analyzed to determine the impact of farrerol on ClpP protein conformation. Additionally, the number of hydrogen bonds formed between the receptor protein and the ligand molecule was monitored over the simulation period. The last 50-ns trajectories of the steady state were used to calculate the binding free energy *via* the MM-GBSA method.

$$\Delta G_{bind} = G_{complex} - G_{protein} - G_{ligand}$$

Where ΔG_{bind} is the binding free energy; $G_{complex}$, $G_{protein}$ and G_{ligand} are the free energies of the complex, protein, and ligand, respectively[24].

2.19 G. mellonella infection experiment

To assess the effectiveness of farrerol against systemic infection in *G. mellonella*, larvae were initially disinfected with 70% ethanol. Following disinfection, the larvae were injected with a 10 μL suspension of MRSA (1×10^7 CFU/larvae) into the last left proleg. After allowing a 1-hour period for infection to establish, the larvae received a 10 μL injection of farrerol at varying concentrations of 20 or 40 mg/kg (1% DMSO + PBS). Each experimental group comprised 15 larvae, with 10 designated for survival analysis and 5 reserved for bacterial quantification and melanin production evaluation. For the survival rate experiment, each *G. mellonella* strain was infected with 1×10^6 CFU of *S. aureus*.

At 4 h postinfection, the bacterial load was determined by counting colony-forming units (CFUs) from five larvae in each group. Hemolymph was collected, appropriately diluted, and plated onto TSBA plates to assess bacterial colony counts. Larval survival rates were recorded every 24 h for a total of 120 h.

2.20 Statistical analysis

All experiments were independently repeated 3 times. Statistical comparisons between groups were conducted *via* Student's *t*-test or one-way analysis of variance (ANOVA), and survival curves were analyzed *via* the log-rank test. $P < 0.05$ was considered to indicate statistical significance.

3. Results

3.1 Farrerol as an inhibitor of ClpP

We employed FRET for the initial screening of flavonoid compounds from our laboratory, aiming to identify potential ClpP inhibitors. ClpP, functioning as a protease, hydrolyzes specific peptide sequences. FRET allows real-time monitoring of ClpP activity by detecting shifts in fluorescence intensity, facilitating rapid screening and evaluation of inhibitor efficacy (Fig. 1A). Our screening identified farrerol, which is primarily sourced from the leaves of *Rhododendron* (Fig. 1B, Table S3), as a potent ClpP inhibitor. Farrerol significantly reduced ClpP activity, with an IC_{50} of 19.95 μg/mL (66.43 μmol/L, Fig. 1C). The MIC of farrerol against *S. aureus* USA300 was determined to be 512 μg/mL (Fig. 1D). To evaluate the effect of farrerol on *S. aureus* USA300 growth, we conducted coculture experiments with 32 μg/mL farrerol and monitored bacterial proliferation over time (Fig. 1E). Notably, even at concentrations double the IC_{50}, farrerol did not affect the viability of A549 or L929 cells (Fig. 1F). Additionally, we evaluated the safety of farrerol at doses of 20 and 40 mg/kg using the *G. mellonella* model. Over the course of 5 days, no signs of melanization or mortality were observed in the larvae, indicating that farrerol is well tolerated at these doses (Table S4). These findings suggest that farrerol selectively inhibits ClpP without impairing host cell viability. Its ability to reduce ClpP activity presents a promising strategy for targeting virulence while avoiding the selective pressures associated with bacterial growth inhibition.

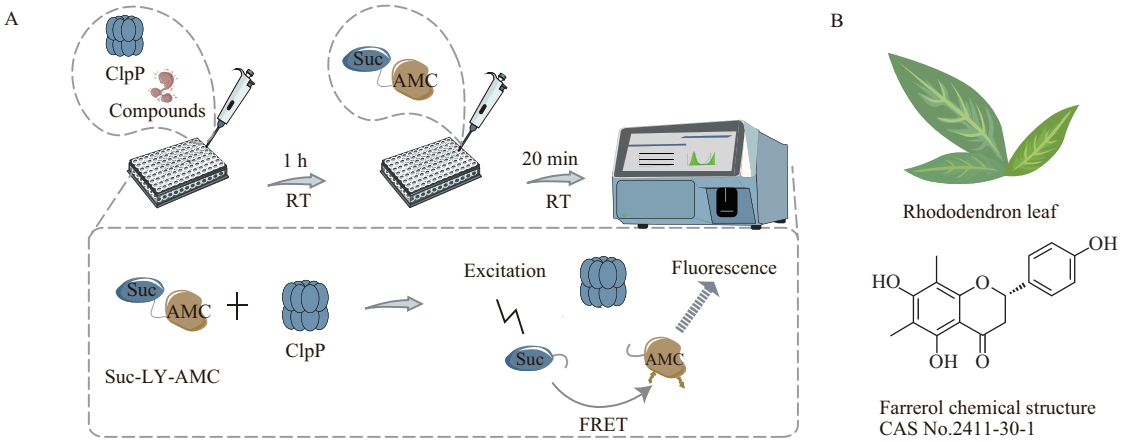

Fig. 1 Identification and evaluation of farrerol as a ClpP inhibitor *via* the FRET method. (A) Schematic representation of the FRET method used to screen flavonoid compounds for ClpP inhibition. FRET enables real-time monitoring of ClpP activity by detecting changes in fluorescence intensity. (B) Chemical structure of farrerol, a flavonoid primarily derived from the leaves of *Rhododendron*. (C) Inhibition curve of ClpP activity by farrerol, showing an IC_{50} value of 19.95 μg/mL (66.43 μmol/L). (D) MIC of farrerol against *S. aureus* USA300 was 512 μg/mL. (E) Growth curve of *S. aureus* USA300 in the presence of 32 μg/mL farrerol, demonstrating no significant effect on bacterial growth over time. Cytotoxicity assay showing that farrerol concentrations ranging from 0 to 32 μg/mL did not affect the growth of (F) A549 and (G) L929 cells. WT, wild-type. n.s. means no signiffcant difference.

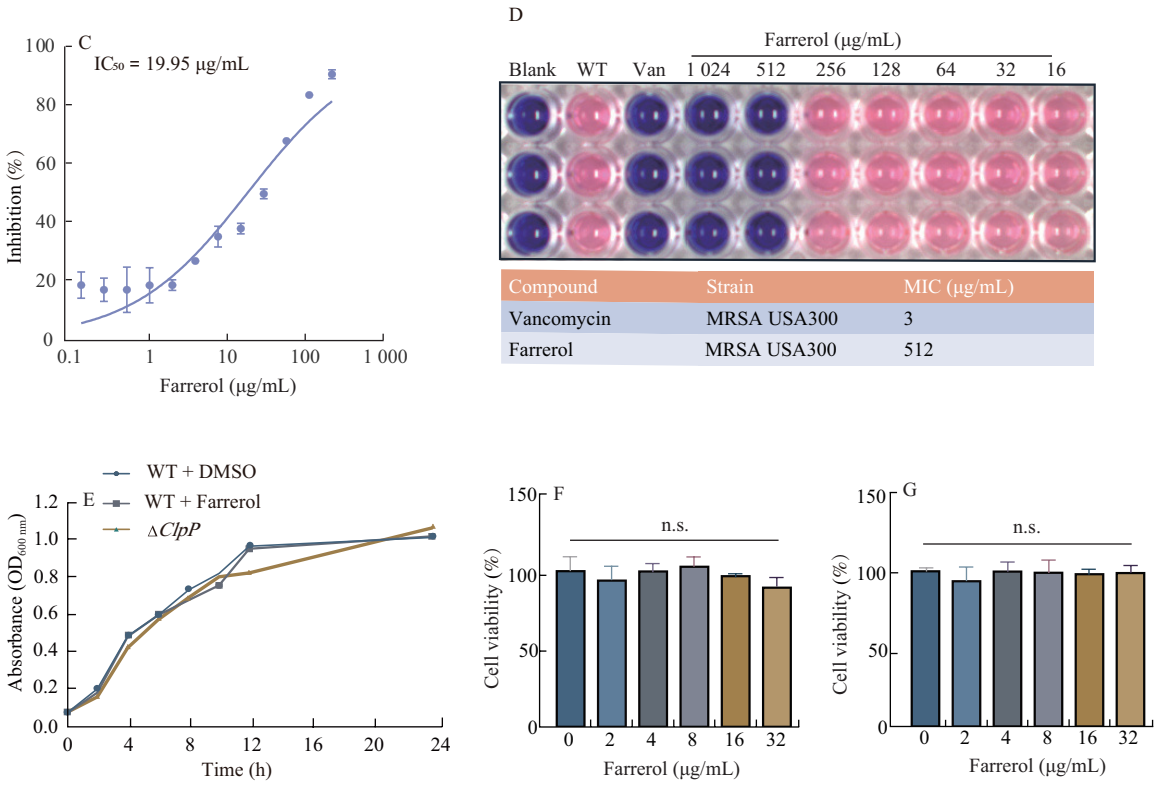

Fig. 1 (*Continued*)

3.2 *Farrerol significantly reduces S. aureus virulence in vitro*

A key aspect of *S. aureus* pathogenicity is its ability to secrete hemolysin (Hla), which significantly damages red blood cells. To investigate this possibility, we first conducted plate hemolysis assays, which revealed that 32 μg/mL farrerol reduced hemolysis, resulting in smaller hemolytic zones. In contrast, the clpP deletion strain exhibited only weak hemolytic activity, with few visible hemolytic zones (Fig. 2A). Additionally, EP tube hemolysis assays demonstrated that farrerol-treated *S. aureus* exhibited a marked reduction in red blood cell lysis, further confirming the inhibition of hemolysis (Fig. 2B).

Further analysis *via* Western blotting of both the supernatant and the bacterial pellet confirmed that farrerol significantly reduced Hla expression levels (Figs. 2C and D), demonstrating its capacity to interfere with key virulence factors. Additionally, our findings revealed that farrerol significantly suppressed PVL production (Fig. 2E), further highlighting its potential to mitigate *S. aureus* virulence. In this study, we focused on the pivotal role of ClpP in the production of *S. aureus* virulence factors. To elucidate this effect, we examined the transcription levels of key virulence genes (such as *RNAIII*, *hla*, *luks*, *psm*, and *spa*) in response to farrerol (32 μg/mL). Through the Agr quorum-sensing system, we observed a significant reduction in the expression of several RNAIII-activated virulence factors, with decreases ranging from 3- to 50-fold. Notably, the transcription levels of critical virulence factors, including *hla*, *luks*, *psm*, and *spa*, particularly the *PVL* gene encoding luksF, were markedly decreased (Fig. 2F).

We also assessed urease activity *via* the use of urease agar base media, as urease is a key component of the acid stress response and a significant virulence factor in *S. aureus*. Farrerol treatment resulted in a color shift to red, indicating increased urease production, suggesting that farrerol disrupts intracellular pH homeostasis, which is potentially mediated by ClpP (Fig. 2G).

These findings highlight the ability of farrerol to attenuate *S. aureus* virulence by targeting ClpP, positioning it as a promising therapeutic agent for managing bacterial infections and preventing immune evasion.

3.3 *Farrerol significantly reduces the invasion of A549 cells by S. aureus*

Adhesion and invasion are critical early steps in the bacterial infection of host cells. To assess the effect of farrerol on *S. aureus* invasion, we used fluorescence microscopy to visualize the bacteria within A549 cells and quantified the number of invasive bacteria *via* agar plate counts (Fig. 3A). In the wild-type (WT) group, a substantial number of FAM-labeled *S. aureus* was detected inside A549 cells, indicating a high level of bacterial invasion. In contrast, the farrerol-treated group presented a significant reduction in the number of internalized bacteria, demonstrating that farrerol effectively inhibits the invasion of A549 cells by *S. aureus*. Similarly, compared with the WT group, the ClpP-deficient group also presented a marked reduction in bacterial invasion.

Quantitative analysis *via* image analysis software further confirmed these findings, revealing significantly fewer FAM-labeled *S. aureus* within A549 cells in both the farrerol-treated and ClpP-deficient groups than in the WT group (Figs. 3B and C). Subsequent analysis following cell lysis supported these results, with

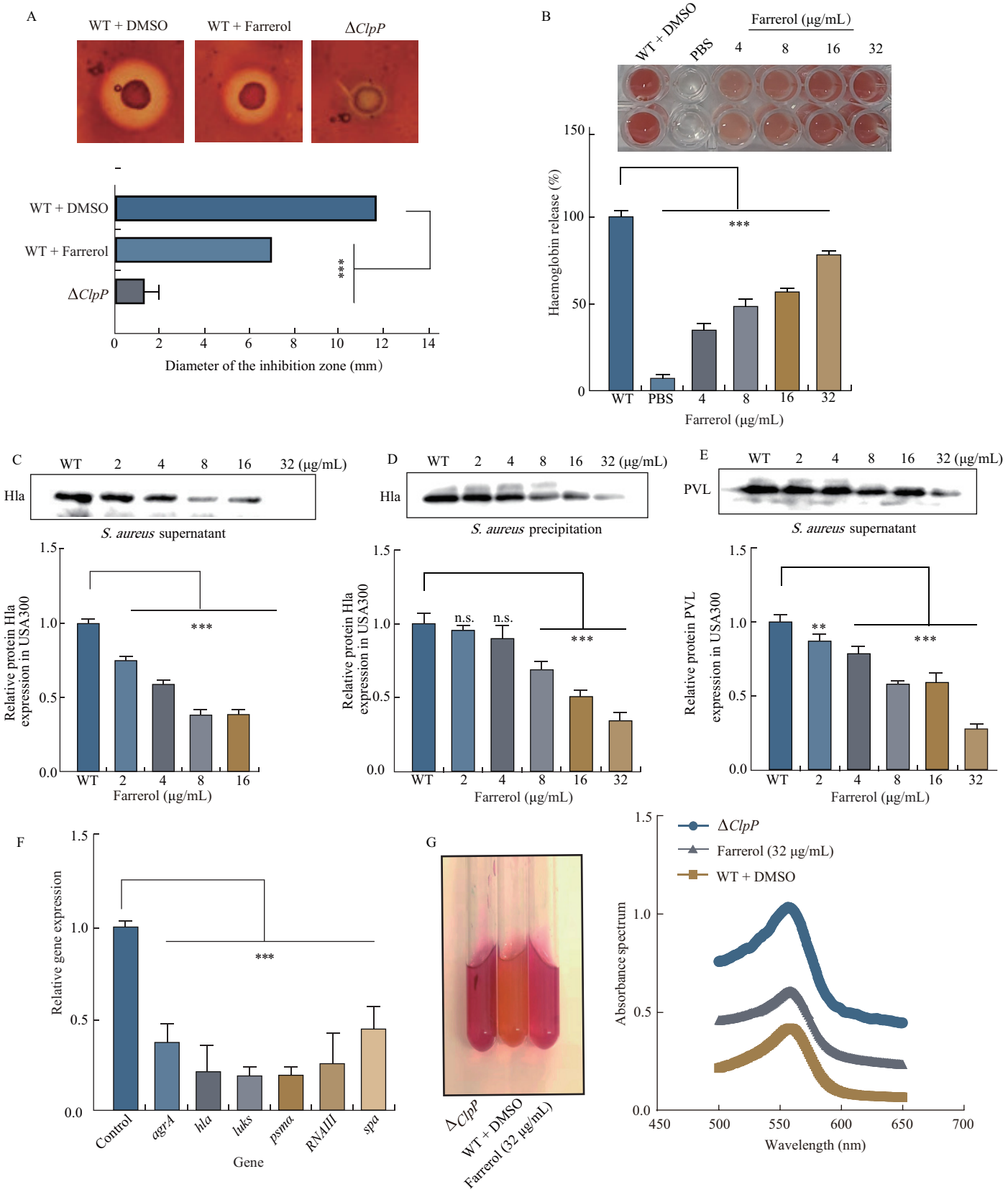

Fig. 2 Farrerol reduces *S. aureus* virulence *in vitro*. (A) Plate hemolysis assays showing reduced hemolysis zones with 32 μg/mL farrerol compared with those of the WT strain. (B) EP tube hemolysis assays demonstrating reduced red blood cell lysis in farrerol-treated *S. aureus*. (C) Western blot analysis of the supernatant showing reduced Hla expression in the farrerol-treated samples. (D) Western blot analysis of the bacterial pellet confirming reduced Hla expression in the farrerol-treated samples. (E) Western blot analysis showing suppressed PVL levels in farrerol-treated *S. aureus*. (F) qPCR analysis of *RNAIII*, *hla*, *luks*, *psm*, and *spa* transcript levels under 32 μg/mL farrerol treatment. (G) Urease activity assay showing increased urease production and disrupted pH homeostasis in farrerol-treated *S. aureus*. WT, wild-type. n.s. means no signiffcant difference, ** $P < 0.01$, ***$P < 0.001$.

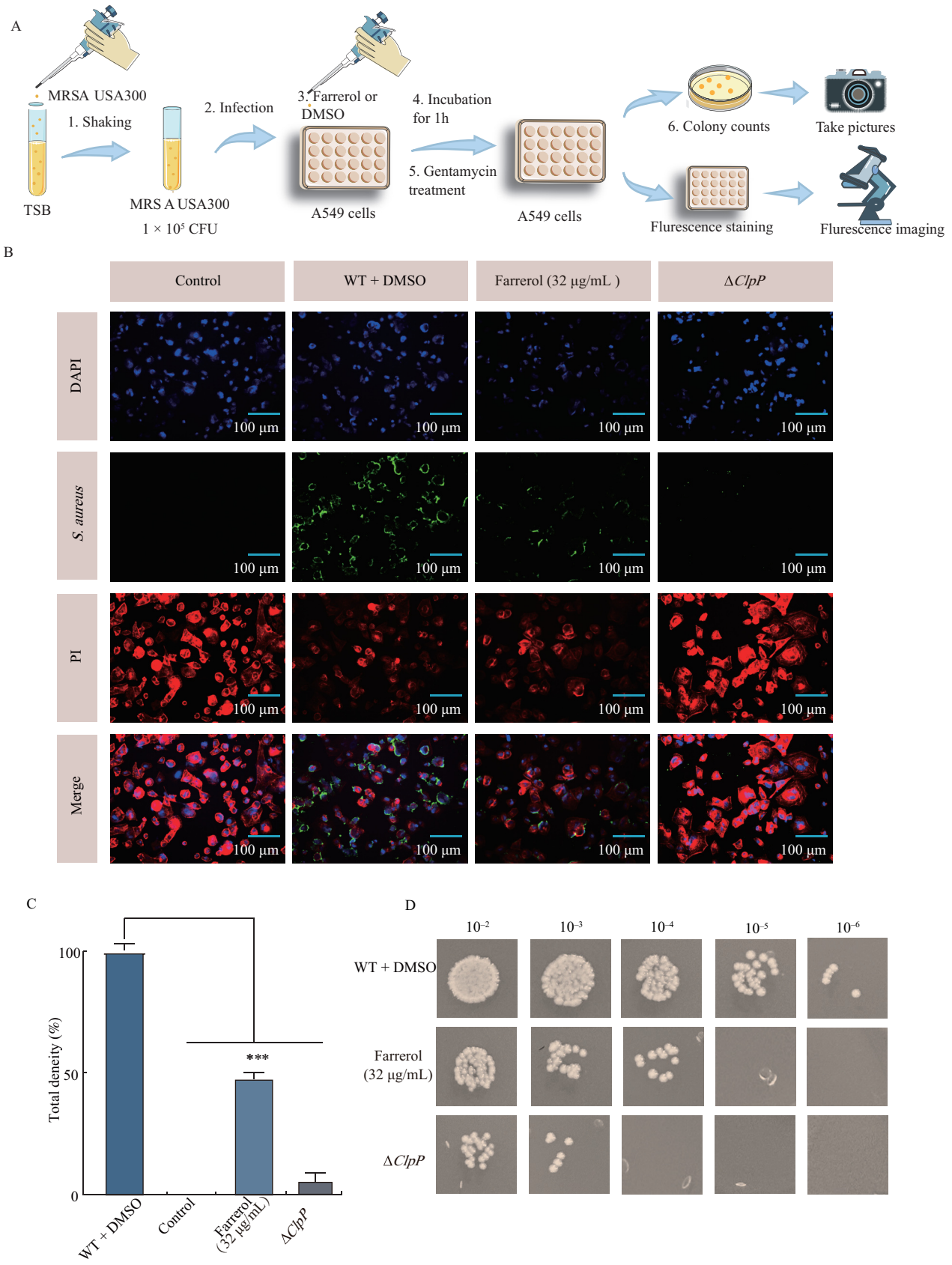

Fig. 3 Farrerol significantly reduced *S. aureus* invasion in A549 cells. (A) Flowchart of the *S. aureus* invasion of A549 cells. (B) Fluorescence microscopy images showing FAM-labeled *S. aureus* within A549 cells, with and without farrerol treatment. (C) Quantitative analysis of internalized FAM-labeled *S. aureus* *via* image analysis software revealed significantly fewer bacteria in the farrerol-treated and ClpP-deficient groups than in the WT group. (D) Quantification of bacteria within A549 cells *via* the plate counting method. ***$P < 0.001$.

the most pronounced reduction in bacterial invasion observed in the ClpP-deficient group, followed by the farrerol-treated group (Fig. 3D). These findings underscore the role of ClpP in the invasion process and highlight the efficacy of farrerol as a potent inhibitor of *S. aureus* invasion.

3.4 Farrerol directly interacts with the ClpP protein

In our study, we further assessed the thermal stability of ClpP to elucidate the interaction between ClpP and farrerol. The results revealed a significant leftward shift of 2 °C in the melting temperature (Tm) of ClpP upon binding with farrerol, indicating reduced thermal stability and confirming a direct interaction (Fig. 4A).

To further verify the intracellular binding of farrerol to ClpP, a CETSA was conducted. In the presence of farrerol, the stability of ClpP decreased with increasing temperature, as evidenced by the reduced band intensity observed *via* SDS-PAGE. This result supports the direct binding interaction observed in the TSA (Figs. 4B and C).

Additionally, fluorescence quenching analysis was performed to further investigate the interaction between farrerol and ClpP. Fluorescence quenching occurs when the intrinsic fluorescence of a protein diminishes owing to structural alterations upon ligand binding. As the concentration of farrerol increased, the fluorescence intensity of ClpP progressively decreased. The K_A was calculated to be 2.810×10^4 L/mol, further confirming the direct interaction between farrerol and ClpP (Fig. 4D).

Moreover, SPR analysis was employed to determine the affinity between ClpP and farrerol. ClpP immobilized on a COOH chip displayed an affinity constant of 78.5 μmol/L for farrerol, as shown by the SPR assay (Fig. 4E). The detailed kinetic affinity results are provided in Table S5.

In conclusion, these findings confirm the strong and specific interaction between farrerol and ClpP, highlighting its potential as a targeted inhibitor.

3.5 Molecular docking and MD simulations of the farrerol and ClpP complexes

To further explore the molecular mechanism underlying the inhibitory effect of farrerol on ClpP, we performed molecular docking studies. Molecular docking provided detailed insights into the interactions between farrerol and ClpP, revealing that farrerol binds to the residues Gly127, Gln132, and Asp170 in the catalytic cavity of ClpP, forming an average of three hydrogen bonds with a docking score of –6.9 kcal/mol, indicating strong affinity (Fig. 5A). The RMSD data indicated that the protein structures of the 2 systems stabilized during the simulation (Fig. 5B). Additionally, the RMSF of ClpP before and

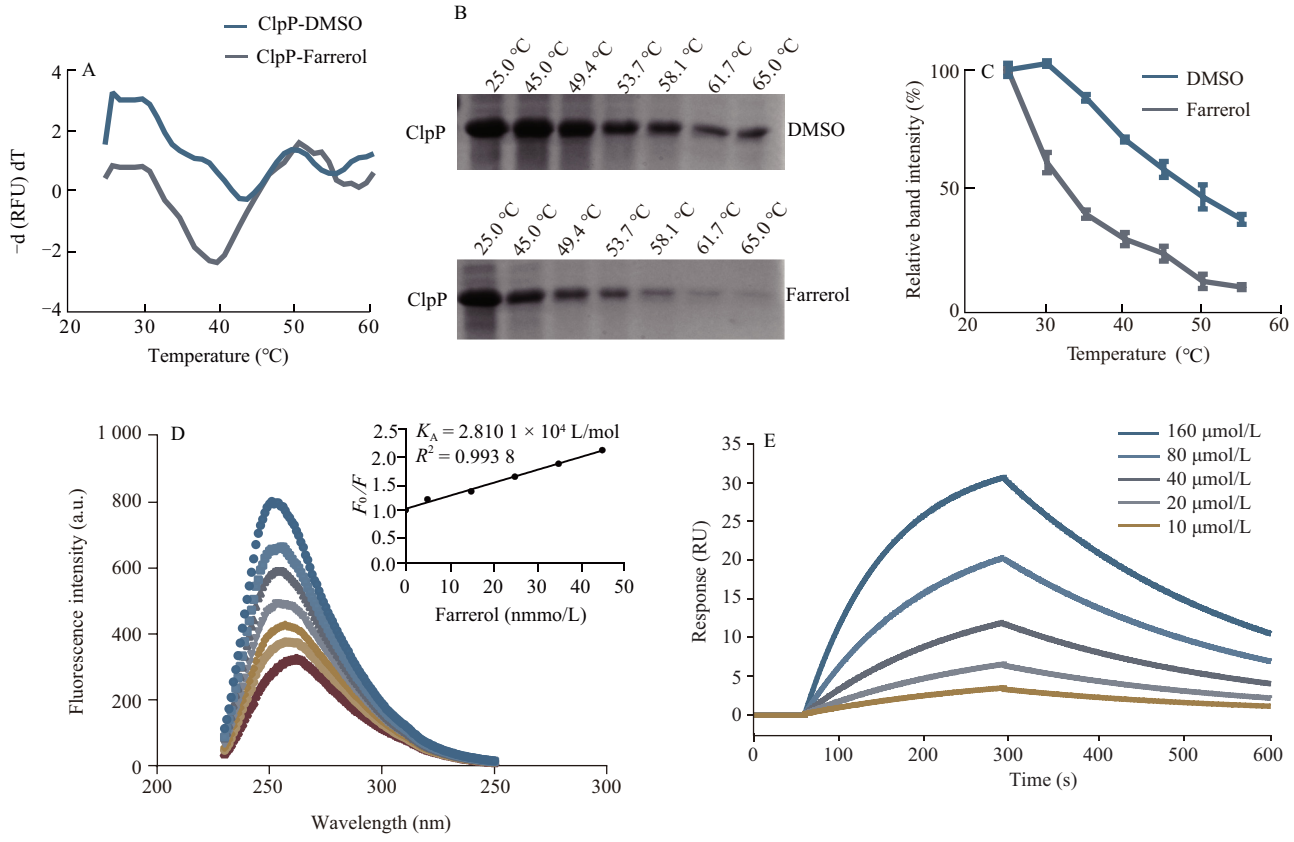

Fig. 4 Farrerol directly interacts with the ClpP protein. (A) TSA showing a significant 2 °C leftward shift in the Tm value of ClpP upon binding with farrerol, indicating reduced thermal stability. (B-C) CETSA demonstrates decreased stability of ClpP at increasing temperatures in the presence of farrerol, confirmed by reduced band intensity on SDS-PAGE. (D) Fluorescence quenching analysis showing a gradual decrease in ClpP fluorescence intensity with increasing farrerol concentration. The K_A was determined to be 2.810×10^4 L/mol. (E) SPR analysis confirming the direct interaction between farrerol and ClpP. The sensorgram clearly demonstrated a binding response, underscoring the specificity of the interaction.

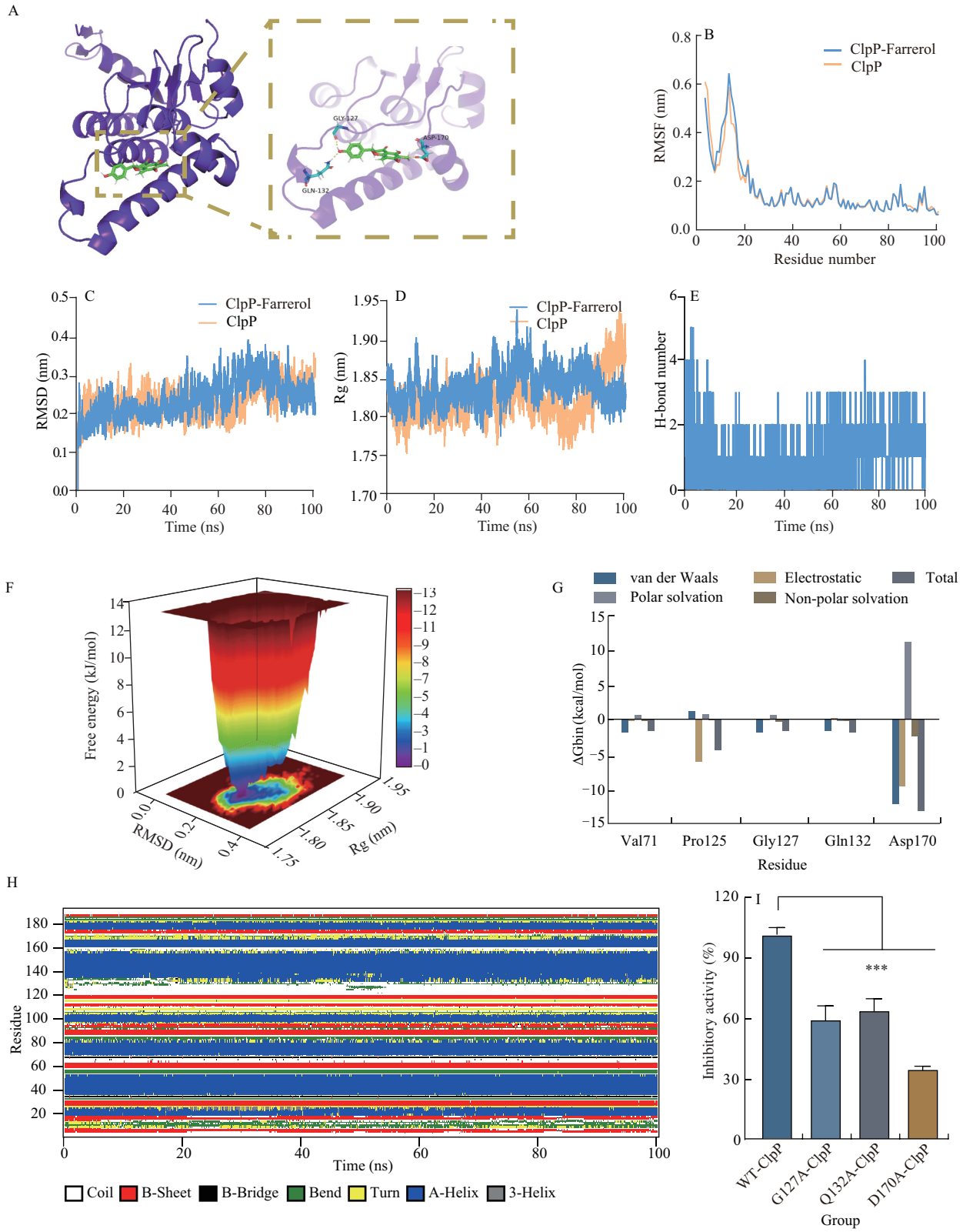

Fig. 5 Molecular docking and MD simulation analysis of the interaction between farrerol and ClpP. (A) Molecular docking study reveals critical binding interactions between farrerol and ClpP, resulting in a docking score of –6.9 kcal/mol. Key residues involved in hydrogen bonding include Gly127, Gln132, and Asp170, which contribute significantly to the stability of the complex. Structural dynamics of the farrerol-ClpP complex are depicted through (B) RMSDs, (C) RMSFs per residue, and (D) Rg, indicating overall stability and compactness of the complex throughout the simulation. (E) Quantification of hydrogen bonds formed between farrerol and ClpP during the MD simulation, highlighting the role of specific interactions in stabilizing the complex. (F) Gibbs energy landscape reveals the most thermodynamically favorable conformational states of the farrerol-ClpP complex, indicating a stable binding conformation. (G) Per-residue binding energy decomposition illustrates the contribution of individual ClpP residues to the total binding energy, with particular emphasis on key interaction hotspots. (H) Analysis of secondary structural changes in ClpP during the MD simulation, demonstrating the impact of farrerol binding on ClpP conformational stability. (I) FRET analysis further confirms the inhibitory effect of farrerol on mutant ClpP proteins, providing insights into its potential to modulate ClpP function.***$P < 0.001$.

after binding with farrerol demonstrated reduced structural flexibility of the loop (Gly127–Asp170) at the entrance of the catalytic cavity (Fig. 5C). The Rg values for the farrerol-ClpP complex ranged from 1.770 90 to 1.934 02 nm, indicating no significant conformational changes in ClpP (1.748 84 to 1.931 49 nm) after binding to farrerol (Fig. 5D). Additionally, the solvent accessible surface area (SASA) plot of the farrerol and ClpP complex is shown in Fig. S2. Hydrogen bonding, a strong noncovalent interaction, was consistently observed, with 2–3 hydrogen bonds forming within 100 ns of the simulation (Fig. 5E). The hydrogen bonds between the ligand and receptor are crucial for maintaining the stability of the complex.

Furthermore, the free energy landscape (FEL) analysis demonstrated a high degree of overlap between the energy minimum conformation and the average conformation, aligning with the RMSD and Rg results (Figs. 5F and S3). To gain more insight into the residues surrounding the binding site and their contribution to the overall system, the electrostatic, van der Waals, solvation, and total contributions of the residues to the binding free energy were calculated *via* the MMGBSA method. Residue Asp170 showed a strong van der Waals interaction with the ligand because of its close proximity to farrerol (Fig. 5G). Additionally, binding to farrerol caused changes in the secondary structure of ClpP, with multiple transitions between turn, bend, and helix structures (Fig. 5H). To further substantiate these findings, the mutant proteins Gly127, Gln132, and Asp170 were engineered and expressed. These mutants retained their ability to cleave the fluorescent substrate Suc-LY-AMC but exhibited resistance to inhibition by farrerol, confirming the involvement of these residues in the binding process (Fig. 5I).

In summary, our molecular docking and dynamics simulations revealed that farrerol binds strongly to the catalytic cavity of ClpP, primarily interacting with Gly127, Gln132, and Asp170, resulting in reduced structural flexibility and stable complex formation. These findings were further confirmed by mutant studies, highlighting the critical role of these residues in the inhibitory effect of farrerol on ClpP.

3.6 *G. mellonella* model demonstrates anti-MRSA activity of farrerol

In this study, we utilized the *G. mellonella* larvae model to evaluate the anti-MRSA activity of farrerol against MRSA USA300. Over a period of 5 days, farrerol was administered to the larvae, and key indicators such as the survival rate, coloration, and bacterial load were closely monitored to determine the therapeutic effectiveness of the compound (Fig. 6A). As shown in Fig. 6B, the infected, untreated group experienced a sharp decline in survival to 10% and exhibited pronounced melanization. In contrast, treatment with farrerol at doses of 20 or 40 mg/kg significantly improved survival rates to 40% and 60%, respectively, with the 40 mg/kg dose resulting in a notable reduction in melanization (Fig. 6C).

Additionally, we assessed the effect of farrerol on the bacterial burden within the larvae. After administering a low dose of MRSA followed by various concentrations of farrerol, we observed a significant decrease in bacterial counts in the larvae 48 h postinfection. The most substantial reduction was observed at the 40 mg/kg dose, highlighting the potent efficacy of farrerol in combating MRSA infections (Fig. 6D).

In conclusion, our findings demonstrate that farrerol has strong anti-MRSA activity in the *G. mellonella* larval model. Treatment with farrerol not only improved survival and reduced melanization but also significantly decreased the bacterial load. These results suggest that farrerol holds promise as a potential therapeutic agent for the treatment of MRSA infections.

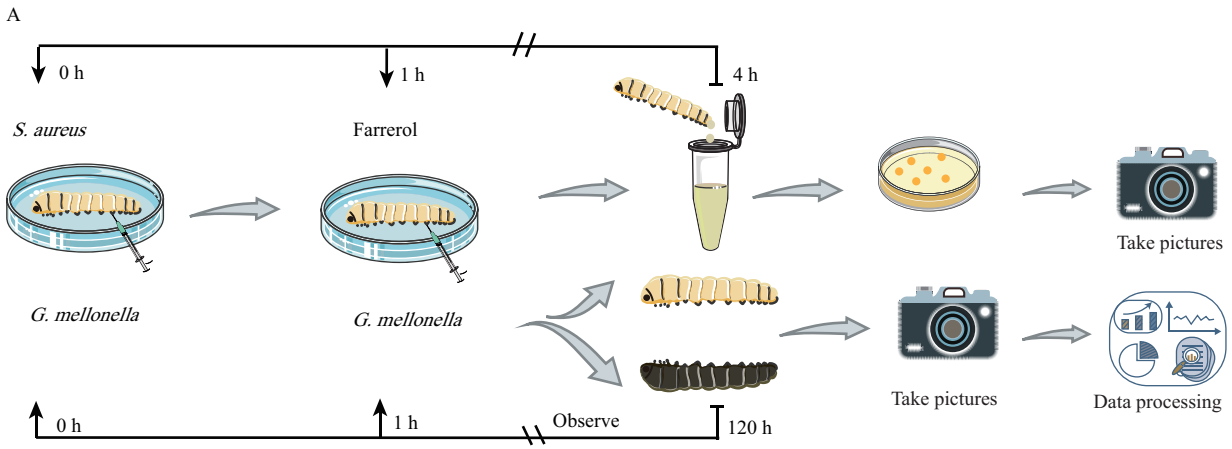

Fig. 6 Evaluation of the anti-MRSA efficacy of farrerol in *Galleria mellonella* infection model. (A) Schematic representation of the experimental setup used to assess the anti-MRSA activity of farrerol in *G. mellonella* larvae. Larvae were infected with MRSA USA300 and treated with farrerol at doses of 20 and 40 mg/kg, administered *via* injection. Over 5 days, key parameters such as survival rate, physical changes (including coloration and melanization), and bacterial burden were monitored to evaluate the therapeutic effects. (B) Kaplan-Meier survival curves for *G. mellonella* larvae over 5 days postinfection, with four experimental groups: untreated (MRSA + PBS + 1% DMSO), farrerol-treated at 20 mg/kg, farrerol-treated at 40 mg/kg, and an uninfected control group. The survival data highlight the dose-dependent protective effects of farrerol against MRSA infection. (C) Visual documentation of the larvae in each group, showing physical changes such as melanization, which correlates with infection severity, and the improvement observed in the farrerol-treated groups. (D) Bacterial load quantification in *G. mellonella* 48 h postinfection. Hemolymph was collected from each group of larvae, serially diluted, and plated on tryptic soy agar, with the bacterial burden measured as CFUs. Farrerol treatment significantly reduced bacterial load in a dose-dependent manner, suggesting potent antimicrobial activity *in vivo*.*$P < 0.05$, ***$P < 0.001$.

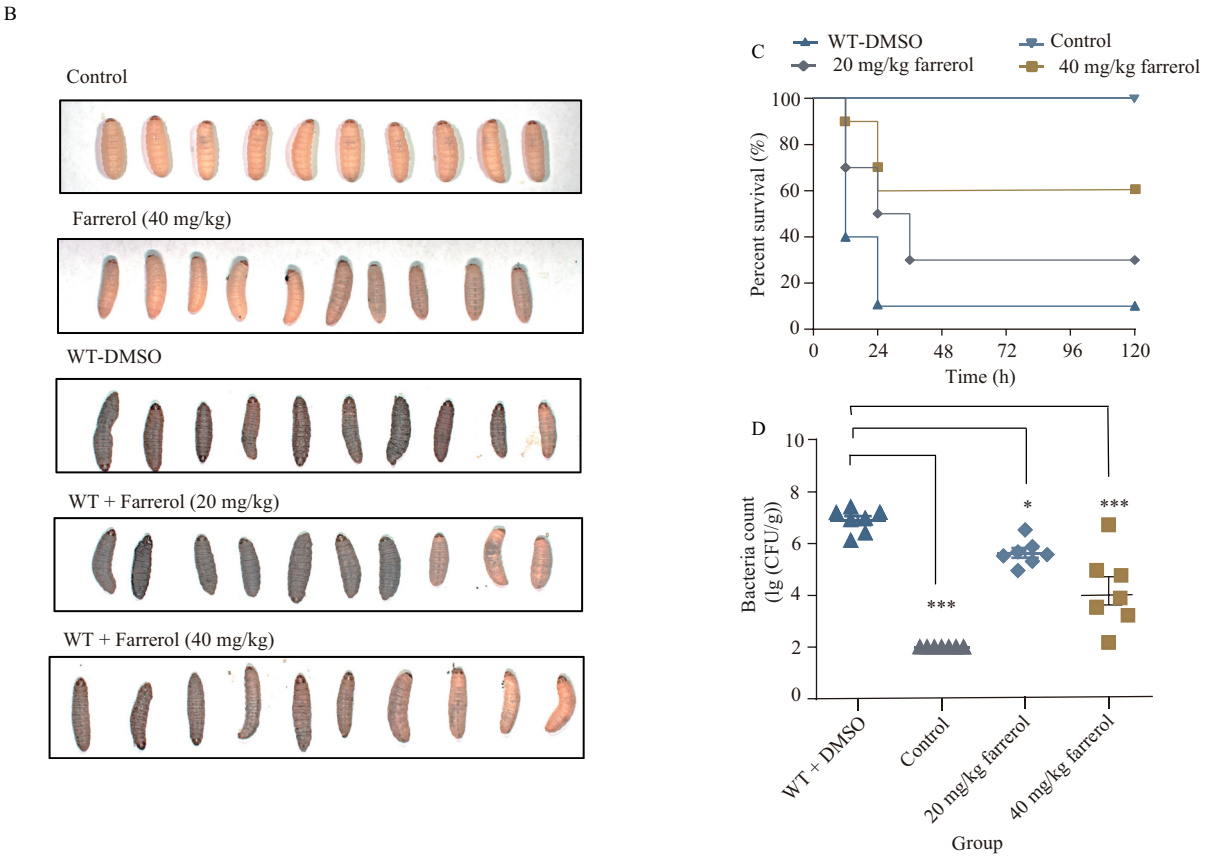

Fig. 6 (*Continued*)

4. Discussion

The improper use of antimicrobial agents in recent years has significantly threatened food safety and public health. The emergence of antibiotic-resistant bacteria due to the overuse and misuse of antibiotics has necessitated the exploration of alternative therapeutic strategies. As a novel approach, antivirulence therapy has gained global attention and has demonstrated considerable development potential[14,25]. Unlike traditional antibiotics that target bacterial growth, antivirulence therapies focus on disarming pathogens by inhibiting their virulence factors, thereby neutralizing their ability to cause disease without exerting selective pressure for resistance development.

One promising target for antivirulence therapy is the ClpP proteolytic complex, a highly conserved multimeric serine protease in bacteria and human mitochondria. ClpP plays a pivotal role in degrading misfolded or damaged proteins involved in various cellular processes, including stationary phase adaptation, nutrient starvation, heat stress response, biofilm formation, cell motility, cell cycle progression, and metabolism. In *S. aureus*, ClpP is crucial for virulence regulation, particularly during the initial phase of pathogenic adhesion[20,26]. Virulence regulation by ClpP in *S. aureus* involves the upregulation of transcriptional repressors of the sarA family and the downregulation of the agr quorum-sensing system[20]. Therefore, inhibitors targeting ClpP are essential for reducing the virulence of pathogenic bacteria and maintaining bacterial homeostasis[17].

Our findings reveal the potential of farrerol, a flavonoid compound, as a novel therapeutic agent that targets the virulence of foodborne pathogens, specifically *S. aureus*. By inhibiting ClpP, farrerol significantly reduces the pathogenicity of *S. aureus* without affecting its growth at concentrations that inhibit ClpP. This antivirulence strategy offers several advantages over traditional antimicrobial approaches.

First, targeting virulence factors such as Hla and PVL significantly impairs *S. aureus*'s ability to invade host cells, evade the immune system, and cause tissue damage[14,27-29]. Hla, or α-hemolysin, is a pore-forming toxin that lyses host cells, including erythrocytes, epithelial cells, and immune cells, contributing to tissue damage and immune system evasion. PVL, another key virulence factor, is responsible for the destruction of leukocytes and further assists in immune evasion. Our results demonstrated that farrerol markedly reduced Hla and PVL expression and activity, as confirmed by hemolysis assays and Western blot analyses. These findings suggest that farrerol disrupts bacterial virulence, thereby reducing the pathogen's ability to cause severe infections. In addition, invasion assays confirmed that farrerol inhibited *S. aureus*'s ability to invade A549 cells, underscoring its efficacy in targeting essential virulence mechanisms.

Second, focusing on virulence inhibition rather than bacterial eradication minimizes the selective pressure that often leads to the development of antibiotic resistance. This approach is particularly advantageous for foodborne pathogens, where antibiotic overuse in agriculture and food production has contributed to resistant strains. Our study revealed that farrerol-treated *S. aureus* did not exhibit growth inhibition at concentrations sixteen times greater than the IC_{50},

highlighting its potential for use in combination with other treatments without inducing resistance. These results support the use of antivirulence strategies such as farrerol as a promising avenue to combat infections while mitigating the risk of antibiotic resistance development.

Moreover, comprehensive analyses of the interaction of farrerol with ClpP *via* methods such as FRET, TSA, CETSA, fluorescence quenching, and molecular docking have provided a thorough understanding of its mechanism of action. The identification of key residues involved in farrerol binding and the construction of resistant mutants underscore the specificity and effectiveness of farrerol in targeting ClpP. These insights pave the way for the development of more targeted and efficient antivirulence therapies.

The *G. mellonella* model offers several advantages over traditional mammalian models. It is cost-effective, ethically favorable, and allows for rapid and high-throughput screening[30-32]. Additionally, the immune response of *G. mellonella* shares several similarities with the innate immune system of mammals, providing relevant insights into host-interactions and the therapeutic potential of anti-infective agents. These advantages make *G. mellonella* an excellent model for preliminary *in vivo* assessments of novel antimicrobial compounds. Our study extends beyond *in vitro* findings by evaluating the therapeutic efficacy of farrerol in an *in vivo* model using *G. mellonella* larvae infected with *S. aureus*. Treatment with farrerol resulted in a significant reduction in the bacterial load within the infected larvae, demonstrating its potent antivirulence activity in a living host.

5. Conclusion

Our research demonstrated that farrerol is a potent inhibitor of *S. aureus* virulence *in vitro* and validated its therapeutic efficacy *in vivo*. By significantly reducing the bacterial load and improving infection outcomes in the *G. mellonella* model, farrerol has emerged as a promising candidate for novel antivirulence treatments. By mitigating the virulence of pathogens such as *S. aureus*, the severity and incidence of foodborne illnesses can be substantially reduced. This strategy not only enhances food safety but also aligns with global initiatives to minimize antibiotic usage and curb antimicrobial resistance. The integration of farrerol into food safety measures and treatment regimens could result in dual benefits: infection control and preservation of the efficacy of existing antibiotics. As we advance, exploring the mechanism of action of farrerol across different bacterial strains and foodborne pathogens, as well as its potential in clinical trials, could pave the way for innovative interventions that increase global public health and food safety standards.

Declaration of interests

The authors declare that they have no known competing financial interests or personal relationships that could have appeared to influence the work reported in this paper.

Acknowledgments

This work was supported by the Jilin Provincial Natural Science Foundation (20220101286JC), and the National Natural Science Foundation of China, General Program (32273058).

Appendix A. Supplementary data

Supplementary data associated with this article can be found, in the online version, at http://doi.org/10.26599/FSHW.2024.9250429.

References

[1] C. Liu, Y. Shen, M. Yang, et al., Hazard of *Staphylococcal enterotoxins* in food and promising strategies for natural products against virulence, J. Agric. Food Chem. 70 (2022) 2450-2465. https://doi.org/10.1021/acs.jafc.1c06773.

[2] Y. Guo, G. Song, M. Sun, et al., Prevalence and therapies of antibiotic-resistance in *Staphylococcus aureus*, Front. Cell Infect. Microbiol. 10 (2020) 107. https://doi.org/10.3389/fcimb.2020.00107.

[3] S. Ryu, M. Shin, B. Yun, et al., Bacterial quality, prevalence of pathogens, and molecular characterization of biofilm-producing *Staphylococcus aureus* from Korean dairy farm environments, Animals 11 (2021) 1306. https://doi.org/10.3390/ani11051306.

[4] Y. Wu, L. Jiang, W. Ran, et al., Antimicrobial activities of natural flavonoids against foodborne pathogens and their application in food industry, Food Chem. 460 (2024) 140476. https://doi.org/10.1016/j.foodchem.2024.140476.

[5] J.Y. Bae, Y.H. Seo, S.W. Oh, Antibacterial activities of polyphenols against foodborne pathogens and their application as antibacterial agents, Food Sci. Biotech. 31 (2022) 985-997. https://doi.org/10.1007/s10068-022-01058-3.

[6] F.Z. El Ftouhy, S. Nassik, S. Nacer, et al., Bacteriological quality of table eggs in moroccan formal and informal sector, Intern. J. Food Sci. 2022 (2022) 6223404. https://doi.org/10.1155/2022/6223404.

[7] G. Blaiotta, D. Ercolini, C. Pennacchia, et al., PCR detection of staphylococcal enterotoxin genes in *Staphylococcus* spp. strains isolated from meat and dairy products. Evidence for new variants of seG and seI in *S. aureus* AB-8802, J. Appl. Microbiol. 97 (2004) 719-730. https://doi.org/10.1111/j.1365-2672.2004.02349.x.

[8] A.E. Mather, M.W. Gilmour, S.W.J. Reid, et al., Foodborne bacterial pathogens: genome-based approaches for enduring and emerging threats in a complex and changing world, Nat. Rev. Microbiol. 22 (2024) 543-555. https://doi.org/10.1038/s41579-024-01051-z.

[9] B.B. Asiimwe, R. Baldan, A. Trovato, et al., Prevalence and molecular characteristics of *Staphylococcus aureus*, including methicillin resistant strains, isolated from bulk can milk and raw milk products in pastoral communities of South-West Uganda, BMC Infect Dis. 17 (2017) 422. https://doi.org/10.1186/s12879-017-2524-4.

[10] X. Kou, H. Cai, S. Huang, et al., Prevalence and characteristics of *Staphylococcus aureus* isolated from retail raw milk in Northern Xinjiang, China, Front. Microbiol. 12 (2021) 705947. https://doi.org/10.3389/fmicb.2021.705947.

[11] F. Gizaw, T. Kekeba, F. Teshome, et al., Multidrug-resistant *Staphylococcus aureus* strains thrive in dairy and beef production, processing, and supply lines in five geographical areas in ethiopia, Veterinary Sci. 10 (2023) 663. https://doi.org/10.3390/vetsci10120663.

[12] S. Escaich, Antivirulence as a new antibacterial approach for chemotherapy, Curr. Opin. Chem. Biol. 12 (2008) 400-408. https://doi.org/10.1016/j.cbpa.2008.06.022.

[13] C. Jenul, A.R. Horswill, Regulation of *Staphylococcus aureus* virulence, Microbiol. Spectr. 1 (2018) 96448632. https://doi.org/10.1128/microbiolspec.GPP3-0031-2018.

[14] S.C. Wu, F. Liu, K. Zhu, et al., Natural products that target virulence factors in antibiotic-resistant *Staphylococcus aureus*, J. Agr. Food Chem. 67 (2019) 13195-13211. https://doi.org/10.1021/acs.jafc.9b05595.

[15] C.P. Gordon, P. Williams, W.C. Chan, Attenuating *Staphylococcus aureus* virulence gene regulation: a medicinal chemistry perspective, J. Med. Chem. 56 (2013) 1389-1404. https://doi.org/10.1021/jm3014635.

[16] F. Ye, J. Li, C.G. Yang, The development of small-molecule modulators for ClpP protease activity, Mol. Biosyst. 13 (2016) 23-31. https://doi.org/10.1039/c6mb00644b.

[17] C. Moreno-Cinos, K. Goossens, I.G. Salado, et al., ClpP protease, a promising antimicrobial target, Int. J. Mol. Sci. 20 (2019) 2232. https://doi.org/10.3390/ijms20092232.

[18] M.E. Aljghami, M.M. Barghash, E. Majaesic, et al., Cellular functions of the ClpP protease impacting bacterial virulence, Front. Mol. Biosci. 9 (2022) 1054408. https://doi.org/10.3389/fmolb.2022.1054408.

[19] A. Michel, F. Agerer, C.R. Hauck, et al., Global regulatory impact of ClpP protease of *Staphylococcus aureus* on regulons involved in virulence, oxidative stress response, autolysis, and DNA repair, J. Bacteriol. 188 (2006) 5783-5796. https://doi.org/10.1128/jb.00074-06.

[20] D. Frees, K. Sørensen, H. Ingmer, Global virulence regulation in *Staphylococcus aureus*: pinpointing the roles of ClpP and ClpX in the *sar/agr* regulatory network, Infect. Immun. 73 (2005) 8100-8108. https://doi.org/10.1128/iai.73.12.8100-8108.2005.

[21] P. Gao, P.L. Ho, B. Yan, et al., Suppression of *Staphylococcus aureus* virulence by a small-molecule compound, PNAS 115 (2018) 8003-8008. https://doi.org/10.1073/pnas.1720520115.

[22] H. Zhang, J. Yan, Y. Zhuang, et al., Anti-inflammatory effects of farrerol on IL-1β-stimulated human osteoarthritis chondrocytes, European J. Pharm. 764 (2015) 443-447. https://doi.org/10.1016/j.ejphar.2015.07.012.

[23] X. Qin, X. Xu, X. Hou, et al., The pharmacological properties and corresponding mechanisms of farrerol: a comprehensive review, Pharm. Bio. 60 (2022) 9-16. https://doi.org/10.1080/13880209.2021.2006723.

[24] J. Shen, W. Zhang, H. Fang, et al., Homology modeling, molecular docking, and molecular dynamics simulations elucidated *α*-fetoprotein binding modes, BMC bioinformatics 14 Suppl (2013) S6. https://doi.org/10.1186/1471-2105-14-s14-s6.

[25] J. Chang, B. Chen, Z. Du, et al., Eugenol targeting CrtM inhibits the biosynthesis of staphyloxanthin in *Staphylococcus aureus*, Food Sci. Hum. Wellness 13 (2024) 1368-1377. https://doi.org/10.26599/FSHW.2022.9250115.

[26] A.Y. Yu, W.A. Houry, ClpP: a distinctive family of cylindrical energy-dependent serine proteases, FEBS Lett. 581 (2007) 3749-3757. https://doi.org/10.1016/j.febslet.2007.04.076.

[27] J. Etienne, Panton-Valentine leukocidin: a marker of severity for *Staphylococcus aureus* infection? Clin. Infect. Dis. 41 (2005) 591-593. https://doi.org/10.1086/432481.

[28] N. Ahmad-Mansour, P. Loubet, C. Pouget, et al., *Staphylococcus aureus* toxins: an update on their pathogenic properties and potential treatments, Toxins 13 (2021) 677. https://doi.org/10.3390/toxins13100677.

[29] B.G.J. Surewaard, A. Thanabalasuriar, Z. Zeng, et al., *α*-Toxin induces platelet aggregation and liver injury during *Staphylococcus aureus* sepsis, Cell Host Microbe 24 (2018) 271-284.e273. https://doi.org/10.1016/j.chom.2018.06.017.

[30] L. Li, H. Chen, Y. Liu, et al., Synergistic effect of linezolid with fosfomycin against *Staphylococcus aureus in vitro* and in an experimental *Galleria mellonella* model, J. Microbiol. Immun. 53 (2020) 731-738. https://doi.org/10.1016/j.jmii.2018.12.007.

[31] A.L. Jorjão, L.D. Oliveira, L. Scorzoni, et al., From moths to caterpillars: ideal conditions for *Galleria mellonella* rearing for *in vivo* microbiological studies, Virulence 9 (2018) 383-389. https://doi.org/10.1080/21505594.2017.1397871.

[32] A.P. Desbois, P.J. Coote, Wax moth larva (*Galleria mellonella*): an *in vivo* model for assessing the efficacy of antistaphylococcal agents, J. Antimicro. Chemoth. 66 (2011) 1785-1790. https://doi.org/10.1093/jac/dkr198.